AGU ADVANCING EARTH AND SPACE SCIENCE

Water Resources Research

RESEARCH ARTICLE
10.1029/2021WR029660

Overtopping-Induced Failure of Non–Cohesive Homogeneous Fluvial Dikes: Effect of Dike Geometry on Breach Discharge and Widening

V. Schmitz[1], S. Erpicum[1], K. El kadi Abderrezzak[2,3], I. Rifai[4], P. Archambeau[1], M. Pirotton[1], and B. Dewals[1]

[1]Research Group of Hydraulics in Environmental and Civil Engineering (HECE), University of Liège, Liège, Belgium, [2]National Laboratory for Hydraulics and Environment (LNHE), EDF R&D, Chatou, France, [3]Saint Venant Laboratory for Hydraulics, Chatou, France, [4]Egis, Guyancourt, France

Key Points:

- Based on laboratory experiments, the influence of dike geometry (channel-side and floodplain-side slopes and crest length) on breach hydrograph and widening has been assessed
- Three types of breach hydrographs have been identified and related to the inflow discharge and the dike geometry
- The conditions of occurrence of the three types of breach hydrographs have been clarified based on a simple conceptual model

Supporting Information:

Supporting Information may be found in the online version of this article.

Correspondence to:

V. Schmitz,
V.Schmitz@uliege.be

Citation:

Schmitz, V., Erpicum, S., El kadi Abderrezzak, K., Rifai, I., Archambeau, P., Pirotton, M., & Dewals, B. (2021). Overtopping-induced failure of non–cohesive homogeneous fluvial dikes: Effect of dike geometry on breach discharge and widening. *Water Resources Research*, *57*, e2021WR029660. https://doi.org/10.1029/2021WR029660

Received 21 JAN 2021
Accepted 23 JUN 2021

Abstract Laboratory experiments were conducted to assess the influence of dike geometry on the breaching of non-cohesive homogeneous fluvial dikes. Both the channel-side and floodplain-side dike slopes and the crest length were varied systematically. The time-evolution of the breach discharge and breach width was monitored. Dikes having a larger volume per unit width lead to a more gradual increase in breach discharge and in breach width during the first stage of breach expansion (i.e., phase of rapid erosion). In contrast, the later stage of gradual breach widening is less influenced by the dike geometry. The breach hydrographs were observed to follow three distinct patterns, which are explained based on the relative magnitude of two characteristic time scales and of a normalized form of the dike unit volume.

Plain Language Summary Fluvial dikes are structures built along rivers to protect population and property from flooding. However, failure of fluvial dikes leads to devastating human, economic and environmental consequences worldwide. Within this context, we conducted laboratory experiments to assess the influence of dike geometry on the breaching of fluvial dikes made out of homogeneous non-cohesive material. The side slopes of a trapezoidal dike and its crest length were varied systematically. The time-evolution of both the breach width and the discharge passing through the breach was recorded. It turned out that dikes having a larger volume per unit width lead to a slower increase in breach discharge and in breach width at the beginning of the experiment (i.e., phase of rapid erosion). In contrast, the rest of the experiment (i.e., phase of gradual breach widening) is less influenced by the dike geometry. It appeared that the breach discharge evolution observed during the different tests follows three distinct patterns, which are explained based on the dike volume per unit width and flow parameters.

1. Introduction

1.1. Context

For millennia, fluvial dikes (also called levees) have been built along long stretches of the world's rivers to protect population and property from flooding (Ward et al., 2017). However, failure of fluvial dikes leads to devastating human, economic, and environmental consequences worldwide (e.g., Bhattarai et al., 2015; LaRocque et al., 2013; Viero et al., 2013; Vorogushyn et al., 2010). The main causes of failure include flow overtopping (Schmocker & Hager, 2009), piping (Vorogushyn et al., 2009), seepage (Michelazzo, Paris, & Solari, 2018), slope instability, and animal burrowing (Orlandini et al., 2015; Viero et al., 2013). Flow overtopping is by far the most frequent cause of failure (Danka & Zhang, 2015; Özer et al., 2020; Zhang et al., 2016). In the following, we focus on overtopping-induced breaching of fluvial dikes.

The risk caused by dike failure is rising due to lack of maintenance, inadequate rehabilitation works and increasingly frequent hydrological extremes, both floods and droughts. Indeed, during prolonged drought periods, cracks may appear in the dike body, thus increasing the failure probability (Van Lanen et al., 2016; Ward et al., 2020). Consequences of dike failure are often magnified by the increase in exposure and socioeconomic activity typically observed in the protected lowlands. This is known as the levee-effect (e.g., Aerts et al., 2018; Di Baldassarre et al., 2018). Therefore, accurately modeling the dike breaching process and the induced flooding is of critical importance for flood risk management. Since field measurements

Table 1
Previous Experimental Research on Overtopping-Induced Breaching of Homogeneous Fluvial Dikes

		Experimental setup				Parameters systematically varied in the tests			
Reference	Laboratory	Dike material	Dike height w (m)	Erodible bottom	Number of tests	Dike composition	Inflow rate Q_{in}	Dike height w	Others
Islam (2012)	Nagoya University	C & NC	0.10–0.20	✓	6	✓	✓	✓[a]	MC bottom elevation
Bhattarai et al. (2015)	Kyoto University	NC (sand)	0.15	✓	21	✓			Bottom erodibility
Charrier (2015)	University of Aix-Marseille	C (clay content)	0.10	–	5	✓	✓		
Yu et al. (2013)	Wuhan University	NC (sand or coal particles)	0.15–0.18	–	12		✓	✓[b]	Curved MC
Wei et al. (2016)	Wuhan University	C	0.16	–	4	✓	✓		Curved MC
Elalfy et al. (2018)	University of South Carolina	NC (sand)	0.20	–	2		✓		
Michelazzo, Oumeraci, and Paris (2018)	LWI Braunschweig	NC (sand)	0.25	✓	10		✓		
Wu et al. (2018)	Wuhan University	NC (sand)	0.15–0.18	–	9	✓	✓	✓[b]	Curved MC
		C (silt loam)	0.18	–	3	✓	✓		
Rifai et al. (2017, 2018)	University of Liege	NC (sand)	0.30	–	23		✓		Backwater effects
Rifai et al. (2021)	EDF R&D, LNHE Chatou	NC (sand and silt)	0.30	–	8	✓	✓		
Present study	University of Liege	NC (sand)	0.30	–	26[c]		✓		L_k, S_u, S_d

Notations and abbreviations: w = dike height; Q_{in} = inflow discharge in the main channel; L_k = length of dike crest; S_d = slope of the floodplain-side of the dike, S_u = slope of the channel-side of the dike; C = cohesive; NC = non-cohesive; BC = boundary condition; MC = main channel.
[a]The dike height varies as a result of changes in the bottom elevation of the main channel, which may differ from the floodplain elevation.
[b]The main channel is curved, forming a 180° bend. [c]As detailed in Section 2.2, these 26 tests include four repetitions to assess the results reproducibility.

are complex and hazardous while experimental tests are relatively costly, computational models simulating the breaching of fluvial dikes are of prime interest. However, those models are not yet mature (e.g., Dou et al., 2014; Elalfy et al., 2018; Faeh, 2007; Kakinuma & Shimizu, 2014), and more experimental research is needed to unravel the underpinning breaching mechanisms.

1.2. State-of-the-Art

Compared to the case of fluvial dikes, more experimental research has been conducted on the failure of embankment dams, that is, earthen or rockfill structures normal to the main river channel (Amaral et al., 2020; Bento et al., 2017; Coleman et al., 2002; Jandora & Říha, 2008; Morris et al., 2007; Müller et al., 2016; Pickert et al., 2011; Sadeghi et al., 2020; Schmocker & Hager, 2009, 2012; Schmocker et al., 2014; among others). In contrast, studies aiming at a deep understanding of the breaching mechanisms of fluvial dikes developed mostly in the last decade (Table 1). The breaching of fluvial dikes exhibits distinct features than those involved in embankment dams (ASCE/EWRI Task Committee on Dam/Levee Breaching, 2011). This includes complex 3D flow structures involving spiral flow in the breach (Michelazzo et al., 2015), non-symmetric breach expansion and impinging jet erosion (e.g., Elalfy et al., 2018; Kakinuma et al., 2013; Rifai et al., 2017).

Field-scale observations of fluvial dike breaching remain scarce, due to the difficulty in setting up large-scale tests, controlling boundary conditions and recording accurate measurements. To our knowledge, only Kakinuma et al. (2013) conducted four field tests of overtopping of 3 m high dikes made of sand and gravel. The dike composition, crest width, and inflow discharge in the main channel were varied.

Laboratory experiments have enabled parametric studies and more detailed monitoring of overtopping-induced breaching of dikes (Table 1). In these experiments, the considered dikes were homogeneous, and their height ranged between 0.10 and 0.20 m, except for the studies by Rifai et al. (2017, 2018, 2021) who used 0.30 m high dikes. Virtually all studies varied the inflow discharge in the main channel. While in all other tests a straight main channel was considered, the dike was placed along the outer bank of a 180°-bend in the experiments of Yu et al. (2013), Wei et al. (2016) and Wu et al. (2018). Bhattarai et al. (2015), Islam (2012) and Michelazzo, Oumeraci, and Paris (2018) used an erodible bottom in their laboratory setup, enabling the analysis of scouring on the floodplain side of the dike. Rifai et al. (2018) considered a confined floodplain to assess the tailwater effect on breach expansion.

Charrier (2015), Wei et al. (2016) and Wu et al. (2018) studied the failure of dikes made of cohesive material. For non-cohesive material, the influence of the dike composition was analyzed by Bhattarai et al. (2015), Islam (2012), and Wu et al. (2018). Results showed generally faster erosion for tests with coarser grains. Tests by Rifai et al. (2021) involved the breaching of dikes made of sand and silt in various proportions (up to 30% volumetric ratio of silt), indicating a limited influence of the silt content on the overall breach dynamics.

In contrast, the influence of the dike geometry was never investigated systematically. Islam (2012) considered three different dike heights; but these variations were obtained from a change in the main channel bottom elevation with respect to the floodplain level, resulting in a different dike height on the channel-side and on the floodplain-side. Yu et al. (2013) analyzed three distinct dike geometries, but several parameters were changed simultaneously (crest length, slope of dike faces as well as dike composition), so that the results do not enable disentangling the effect of individual geometric parameters. Wu et al. (2018) tested two different relative crest lengths. However, Yu et al. (2013) and Wu et al. (2018) placed the dike in a 180° bend, thus hampering the transposition of their findings to the more canonical case of a fluvial dike along a straight main channel.

1.3. Objective

Knowledge gaps remain regarding how the breaching process is influenced by dike geometric parameters, such as the ratio of the crest length to the dike height (L_K/w), or the channel- and floodplain-side slopes (S_u and S_d, respectively, as shown in Figure 1). The influence of these parameters was studied for the frontal configuration (e.g., Müller et al., 2016), but not for a fluvial dike. In this study, we aim to unveil the impact of variations in the geometry of a non-cohesive dike on the breach widening and outflow hydrograph in case of flow overtopping. Based on the same laboratory setup as used by Rifai et al. (2017, 2018), we present the results of tests covering eight distinct dike geometric configurations, in combination with three inflow discharges in the main channel.

The laboratory setup, test program and measurement techniques are presented in Section 2. Section 3 details the observed evolution of the breach discharge and width. In Section 4, we provide a typology of breach hydrographs and hint at an explanation based on the relative magnitude of two time scales and of the dike normalized unit volume. Conclusions are drawn in Section 5.

2. Laboratory Experiments

2.1. Experimental Setup

The experimental setup was located in the Laboratory of Hydraulic Engineering of the University of Liege (Figure 1). It consists of a horizontal, straight main channel (10 × 1 m) of trapezoidal cross-section, with a 3-m-long lateral opening towards a floodplain (4.3 × 2.5 m). Along this side opening, a trapezoidal-shaped fluvial dike was built with uniform sand of median diameter $d_{50} = 1$ mm, following the same procedure as used by Rifai et al. (2017, 2018, 2019). The main channel and floodplain were covered with an impermeable whitewash coating to ensure roughness continuity between the flume, floodplain, and sand dike (Rifai et al., 2017). The bottom of the main channel and the floodplain were at the same level. To control seepage flow through the dike body, a drainage system was installed at the dike bottom (Rifai et al., 2017, 2019). Finally, a perforated plate followed by a reservoir with a calibrated weir was placed at the main channel

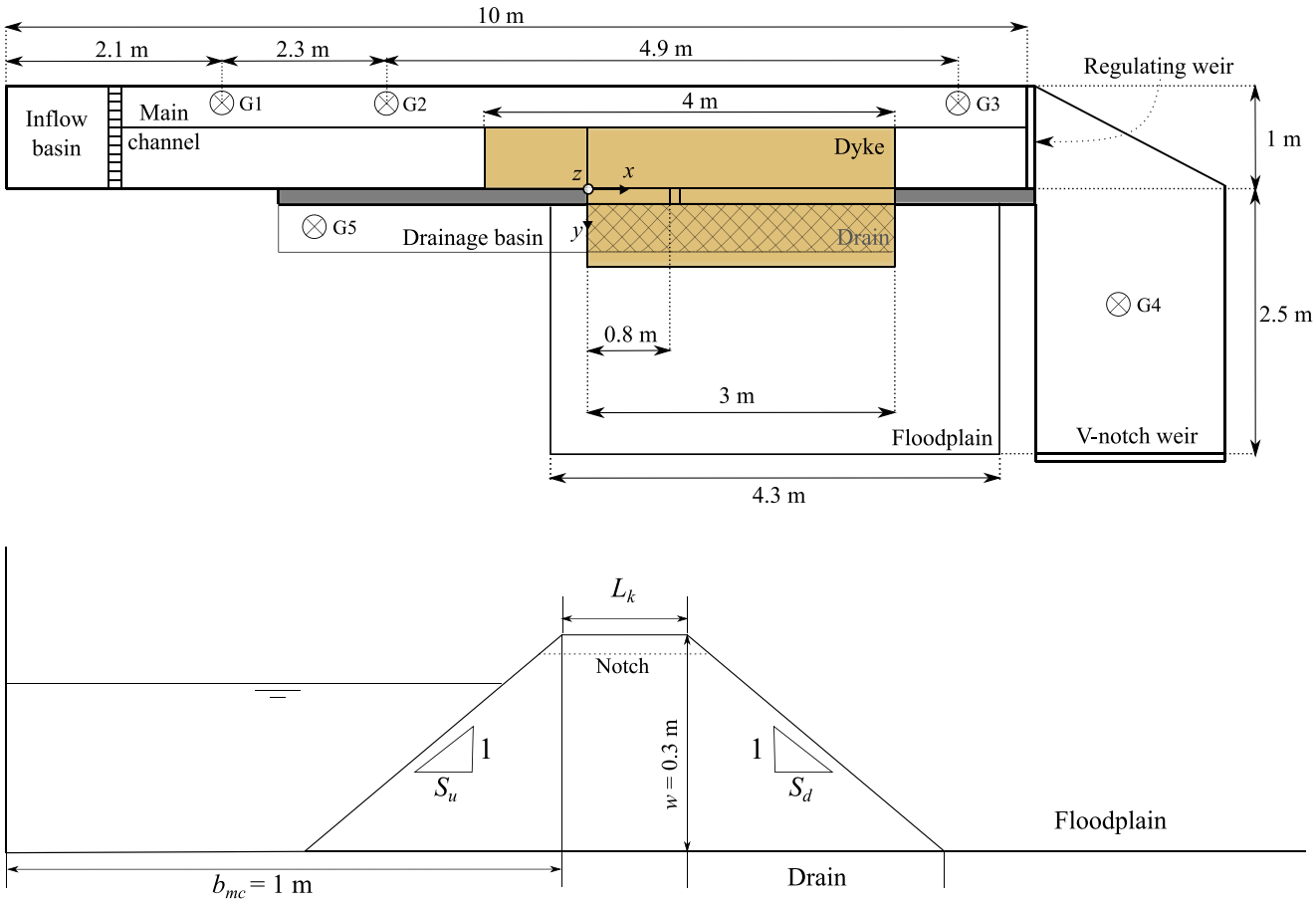

Figure 1. Experimental setup: (a) plane view; (b) dike vertical profile, highlighting main geometric parameters: channel-side and floodplain-side dike slopes (S_u and S_d), height (w), and crest length (L_k).

end to control the downstream water level and collect the main channel outflow. A full description of the laboratory setup was provided by Rifai et al. (2017, 2019).

The dike geometry is characterized by its height w as well as by the channel-side slope S_u, the floodplain-side slope S_d and the crest length L_k (Figure 1b). The dike height was kept constant at $w = 0.3$ m in all tests, while the three other parameters were systematically varied.

Each geometric configuration was tested with three different main channel inflow discharges. The inflow discharge Q_{in} was kept constant and supplied at the main channel upstream end. During the filling phase, the water level rose in the main channel. The perforated plate was adjusted such that, at the beginning of each test, the water level corresponded to the dike crest elevation. To trigger breaching, a 2-cm-deep and 10-cm-wide initial notch was created in the dike crest, at a distance of 0.8 m from its upstream end. Once the water level overtopped the notch, surface erosion and breaching developed.

The primary goal of the present study is to investigate the breaching mechanisms of fluvial dikes, and not to represent a scaled particular field structure. Nonetheless, assuming that material entrainment and failure are dominating processes in the breaching of non-cohesive homogeneous dikes, it is reasonable to consider the similarity of Shields number and of the side slope stability factor in the interpretation of the laboratory tests (El kadi Abderrezzak et al., 2014). Considering the Froude similarity for undistorted moveable model, with a sufficiently high Reynolds number, the grain size scales like the flow depth for alluvial material (i.e., sediment density and angle of repose are almost similar in the model and prototype). Therefore, the current experimental model may be seen as a 1:10 scale model of a 3-m high prototype dike made of medium gravels of 1 cm in diameter.

Table 2
Test program

Conf. ID	S_u (−)	S_d (−)	L_k (m)	μ	Q_{in} (l/s)			F		
A	2.0	2.0	0.15	1	25	40	55	0.083	0.133	0.183
B	1.5	2.0	0.15	0.9	25	40	55	0.071	0.114	0.157
C	2.0	1.5	0.15	0.9	25	40	55	0.083	0.133	0.183
D	2.0	2.5	0.15	1.1	25	40	55	0.083	0.133	0.183
E	2.0	3.0	0.15	1.2	25	40	55	0.083	0.133	0.183
F	2.0	2.0	0.00	0.8	25	40	55	0.083	0.133	0.183
G	2.0	2.0	0.30	1.2	25	40	55	0.083	0.133	0.183
H	2.0	2.0	0.60	1.6	–	–	55	–	–	0.183

Note. The four tests corresponding to underlined values of the inlet discharge Q_{in} were repeated twice to assess the reproducibility of the observations.

2.2. Test Program

The test program is detailed in Table 2. Eight different dike geometries were considered, as well as three different inflow discharges in the main channel: Q_{in} = 25 l/s, 40 l/s, and 55 l/s. A total of 26 experiments were carried out, with four of them aiming at assessing the test reproducibility.

The first configuration (A) leads to non-dimensional geometric parameters identical to those of the reference dike used by Müller et al. (2016): $S_u = S_d = 2$ and $L_k = 0.15$ m (i.e., $L_k/w = 0.5$). This dike geometry is used as a reference here. The seven other geometric configurations were defined by varying one geometric parameter at a time. While the floodplain-side of the dike was varied between $S_d = 1.5$ and $S_d = 3$, the channel-side of the dike was only varied between $S_u = 1.5$ and $S_u = 2.0$ for two reasons. First, tests involving variations in S_u were particularly demanding because they required an adaptation of the main channel cross-section over the whole length of the laboratory setup, whereas varying S_d or L_k implied only a change in the construction of the sandy dike. Second, using $S_u = 3$ would lead to a dike extending over 90% of the main channel width (Figure 1a), which was deemed unrealistic. Configuration H was only tested with Q_{in} = 55 l/s due to difficulties in triggering breaching for this particularly strong (i.e., with a relatively large volume per unit width) dike ($L_k/w = 2$). Table 2 also provides the value of μ, defined as the dike volume per unit width ($L_k\, w + w^2\, (S_u + S_d)/2$) normalized by its value for a dike of identical height w but characterized by the following non-dimensional geometric parameters: $S_u = S_d = 2$ and $L_k/w = 0.5$. This indicator was introduced by Müller et al. (2016) for studying the influence of dam geometry on the breaching in frontal configuration. Table S1 in Supplement details each individual test, highlighting among others small deviations (mean value of 3%) between the target inflow discharge (as mentioned in Table 2) and the actual one. Indeed, in each test, the inflow discharge was slightly adapted compared to its target value, to ensure that the water level in the main channel just exceeds the initial notch level at the beginning of the experiment.

2.3. Measurement Techniques

The water level was measured at three locations in the main channel (G1, G2, and G3), in the outflow tank (G4) and in the drainage tank (G5) using ultrasonic sensors (accuracy of ±1 mm) (Figure 1a). The inflow discharge Q_{in} was measured using an electromagnetic flowmeter (accuracy of ±0.5% of full scale, i.e., 150 l/s). The outflow discharge was deduced from the discharge passing through a V-notch weir (deduced from water level at G4) and mass balance in the outflow tank. The drainage discharge Q_d was estimated from the water level measured at G5. The breach discharge Q_b was determined from mass balance in the main channel (Rifai et al., 2017, 2019).

The experiments were recorded with a digital video camera (Panasonic GH4) set on Full-HD resolution (1,920 × 1,080 pixels) and with a recording speed of 60 frames/s. Compared to previous studies (Table 1), a relatively high number of tests was performed here. To monitor the breach widening, we used a simplified version of the laser profilometry technique presented by Rifai et al. (2020): the laser sheet was not rotated in our case, which enabled us to reliably monitor the breach widening at the crest level as the laser sheet was aligned with the dike crest, but not to produce 3D reconstructions of the breach evolving geometry.

3. Results

Figures 2 and 3 represent the evolution of the breach discharge and of the breach widening for each tested geometric configuration and each inflow discharge in the main channel. The evolution of the water level in the main channel is shown in Figure S1 in Supplement. Snapshots of experimental tests in Configuration A ($S_u = 2$, $S_d = 2$, $L_k = 0.15$ m) at four different times for three inflow discharges are available in Table S3 in Supplement.

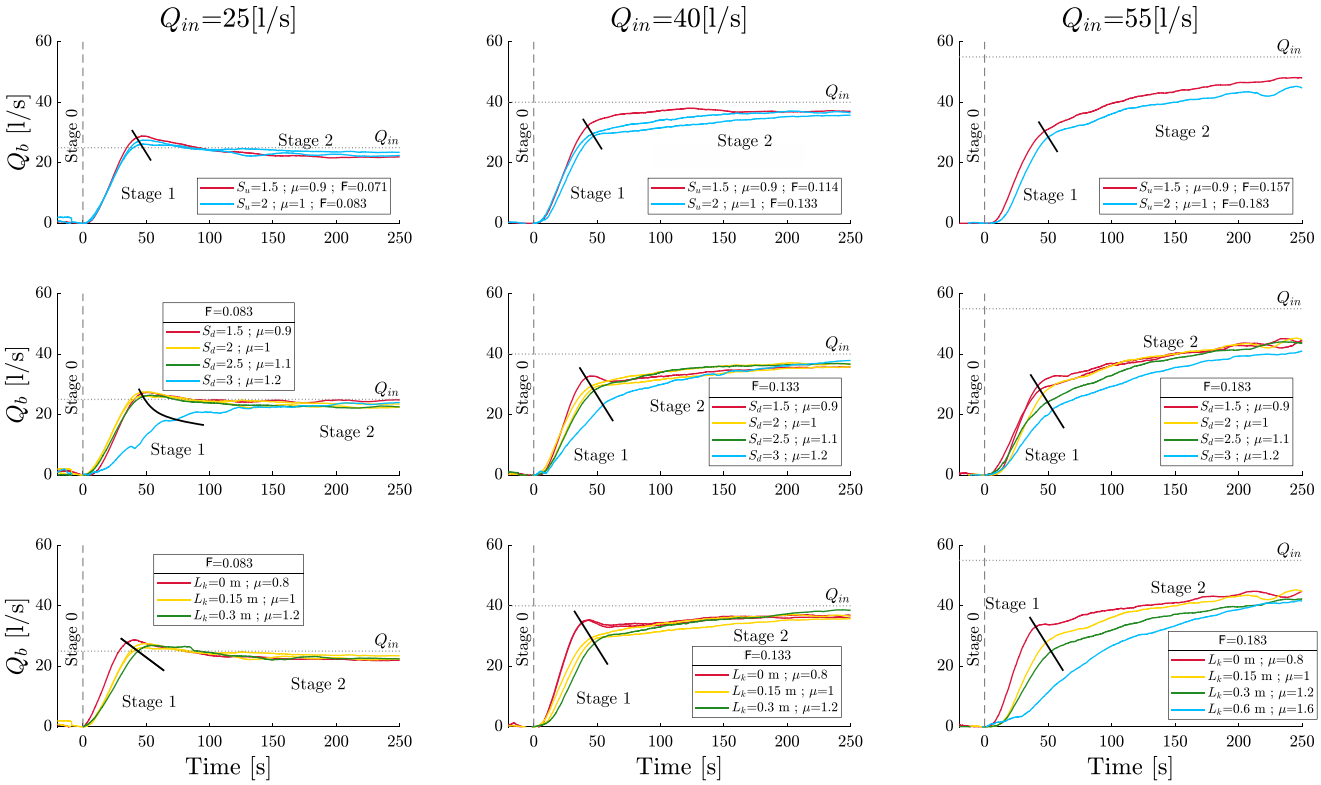

Figure 2. Evolution of the breach discharge Q_b for all tested geometric configurations and inflow discharges. In each plot, values of parameters not specified in the legend are set as in the reference case, that is, Configuration A: $S_u = 2$, $S_d = 2$, $L_k = 0.15$ m. The black lines highlight the transition between Stage 1 and Stage 2. Origin of time corresponds to the start of Stage 1. Curves of identical color in a same panel refer to repeated tests.

3.1. Stages of Breach Expansion

As detailed by Rifai et al. (2017, 2018), the breach evolution can be subdivided into three main stages: gradual start of overtopping at the initial notch, with a slow initiation of dike erosion (Stage 0), rapid erosion, leading to a fast increase in the breach size (width and depth) and discharge (Stage 1), quasi-stabilization of the flow with a reduced flow depth in the main channel and, generally, a continuing but slow breach expansion towards downstream (Stage 2). Note that our analyses do not focus on Stage 0, which is affected by the initial notch characteristics and channel filling procedure.

In Figures 2 and 3, Stages 1 and 2 can be clearly distinguished. Almost all curves start with a steep initial increase in the breach discharge and in the downstream widening, followed by a relatively abrupt slope reduction indicating the transition between Stage 1 and Stage 2. In general, the lower the dike unit volume (i.e., lower values of S_u, S_d or L_k, hence also of μ), the more noticeable the transition between Stage 1 and Stage 2. Only in the case of a particularly strong dike (longest considered crest length: $L_k = 0.6$ m, $\mu = 1.6$) and highest inflow discharge ($Q_{\text{in}} = 55$ l/s), no clear transition can be detected.

In most tests, the breach invert reached the main channel bottom over at least part of the breach width; but this was not the case for the strongest dike (Configuration H, $L_k = 0.6$ m). A more thorough description of the breaching mechanism is provided by Rifai et al. (2017), and is not repeated here for the sake of brevity. The reproducibility of the tests can be assessed by comparing curves of identical color in a same panel in Figures 2 and 3. The relative difference in breach discharge between two repeated tests is lower than 10% of the corresponding inflow discharge, as shown in Figure S2.

3.2. Influence of Dike Geometry in Stage 1

In several cases, a global or a local maximum can be seen in the breach hydrograph (Figure 2). When the inflow discharge is relatively small ($Q_{\text{in}} = 25$ l/s), all hydrographs exhibit a global maximum, except in

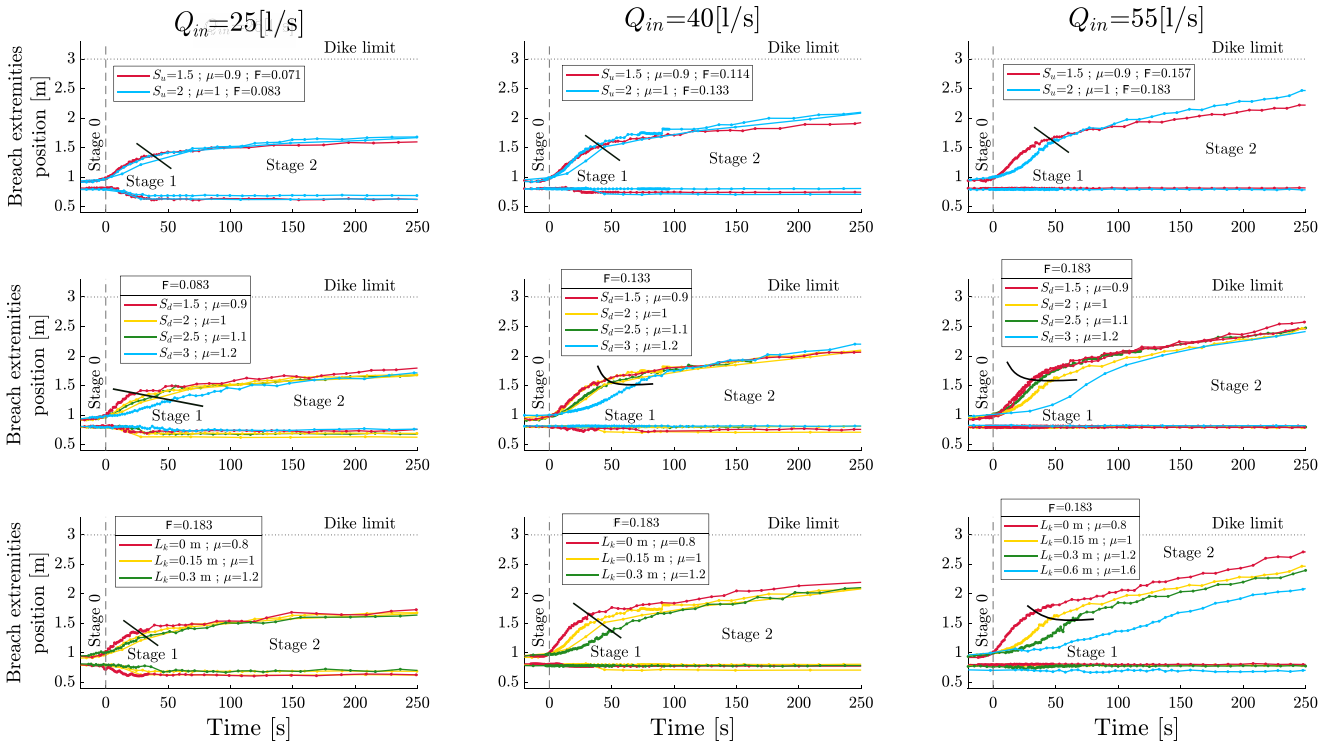

Figure 3. Evolution of the breach extremities location (at the crest level, along the crest center line), with initial notch at $x = 0.8$ m, for all tested geometric configurations and inflow discharges. In each plot, parameters not specified in the legend are set as in the reference case, that is, Configuration A: $S_u = 2$, $S_d = 2$, $L_k = 0.15$ m. The black lines (or curves) highlight the transition between Stage 1 and Stage 2. Origin of time axis corresponds to the start of Stage 1. Curves of identical color in a same panel refer to repeated tests. Data could not be retrieved for one repeated test (Run 8-R in Table S1) in Configuration F ($\mu = 0.8$) with $Q_{in} = 40$ l/s.

Configuration E which corresponds to the strongest dike ($S_d = 3$, $\mu = 1.2$) tested for this value of Q_{in}. Moreover, the weaker the dike, the more pronounced the magnitude of the peak in the breach discharge: the maximum value of the breach discharge reaches about 115% of Q_{in} for $\mu \leq 1$, while the ratio breach discharge Q_b to Q_{in} ranges between 105% and 110% when $\mu > 1$. For a moderate inflow discharge ($Q_{\text{in}} = 40$ l/s), a local maximum can be noticed only for particularly weak dikes, that is, in Configuration C ($S_d = 1.5$, $\mu = 0.9$) and Configuration F ($L_k = 0$ m, $\mu = 0.8$). No maximum in the breach hydrograph is visible for stronger dikes ($\mu \geq 1.0$), nor when the inflow discharge becomes higher ($Q_{\text{in}} = 55$ l/s).

When the inflow discharge is increased, the breach expansion towards downstream intensifies, whereas the expansion towards upstream is reduced (Figure 3). For the highest tested inflow discharge ($Q_{\text{in}} = 55$ l/s), the breach does not expand towards upstream, irrespective of the dike geometry, except for the strongest dike ($L_k = 0.6$ m, $\mu = 1.6$). This appears consistent with the higher flow momentum parallel to the dike axis when $Q_{\text{in}} = 55$ l/s, leading to stronger erosion by impinging jet on the downstream part of the breach, and a gradual shift of the breach centerline towards the channel downstream end.

As can be seen in Figure 2, the gradient in breach discharge during Stage 1 is milder for stronger dikes (i.e., higher values of μ) than for weaker dikes. This influence of the dike geometry on the breach hydrograph is magnified when the inflow discharge is higher. Indeed, the differences between the breach hydrographs are stronger in the cases $Q_{\text{in}} = 55$ l/s than they are for $Q_{\text{in}} = 40$ l/s and for $Q_{\text{in}} = 25$ l/s. These observations are well supported by Figure S3 in Supplement, which plots a characteristic rising time of the breach hydrograph in Stage 1, as a function of the geometric parameters S_u, S_d, L_k and μ: the stronger the dike, the shorter the rising time of the breach hydrograph. The effect of changing S_u seems smaller; but it is certainly due to its smaller range of variation (between 1.5 and 2.0) compared to that of S_d (between 1.5 and 3.0). Also, the change in the rising time with the dike geometry is more pronounced for higher values of Q_{in}. Similarly,

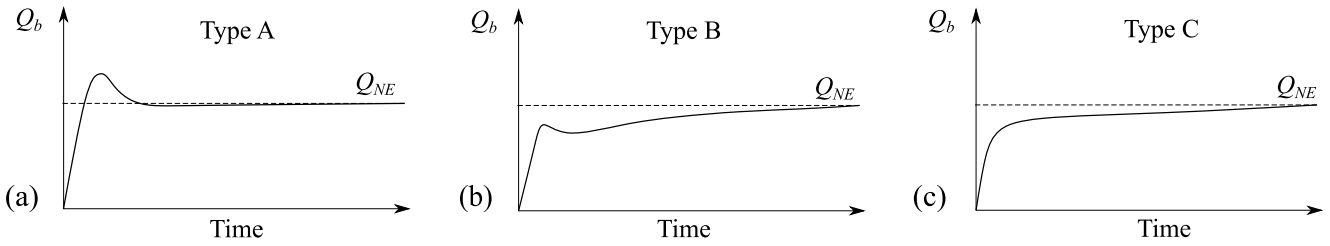

Figure 4. Breach hydrograph types: breach hydrograph with (a) an absolute or (b) relative maximum, and (c) a monotonously increasing breach hydrograph.

Figure 3 reveals that the breach expands faster during Stage 1 in the case of a weaker dike, while for stronger dikes it widens more gently in both up- and downstream directions.

3.3. Influence of Dike Geometry in Stage 2

During Stage 2, the breach expansion rate is less influenced by the dike geometric parameters than it is during Stage 1 (Figure 3). Only variations in the channel-side dike slope S_u seem to have a significant effect on the breach widening rate during Stage 2. This effect is magnified when Q_{in} is increased. However, this may result from the fact that varying the channel-side dike slope S_u while keeping the inflow discharge Q_{in} constant modifies the cross-section in the main channel, and therefore also the flow velocity, the Froude number F and the storage volume in the main channel.

Similarly, the breach discharge in Stage 2 is little affected by the dike geometric characteristics. For relatively low and intermediate inflow discharges in the main channel (Q_{in} = 25 l/s and Q_{in} = 40 l/s), the breach discharge in Stage 2 converges towards a similar value, fairly close to Q_{in}, irrespective of the dike geometry. Figure S4 in Supplement displays the breach hydrographs based on a logarithmic axis for time. This enables a better appraisal of the convergence of the breach discharge towards a quasi-equilibrium value Q_{NE} (Michelazzo, Oumeraci, & Paris, 2018). For Q_{in} = 25 l/s, a quasi-equilibrium breach discharge is reached before the end of the tests, with a value ranging between 90% and 95% of the inflow discharge, regardless of the dike geometric parameters. Similar results are obtained for Q_{in} = 40 l/s, whereas for Q_{in} = 55 l/s the tests were stopped before the breach discharge reached a quasi-equilibrium value, because the downstream breach expansion reached the limit of the 3 m long erodible dike section.

Figure S5 in Supplement represents the quasi-equilibrium breach discharge Q_{NE} (normalized by the inflow discharge Q_{in}) as a function of each geometric parameter (S_u, S_d, L_k) and as a function of the dike volume per unit width (μ). No significant trend can be detected, confirming the limited influence of the dike geometry on Q_{NE} and, more generally on Stage 2 of the breach expansion.

4. Discussion

4.1. Typology of Breach Hydrographs

Based on the results presented in Figures 2 and 3, a standard approach consists in normalizing the observations to derive relationships between non-dimensional variables (e.g., Schmocker & Hager, 2012; Schmocker et al., 2014). In line with this approach, Figure S3 in Supplement suggests that the non-dimensional parameter μ introduced by Müller et al. (2016) succeeds in capturing the overall effect of parameters S_u, S_d and L_k. In contrast, it was not possible to normalize the breach hydrographs so that they feature onto a single curve, because they follow distinct patterns.

The observed breach hydrographs (Figure 2) follow three distinct patterns, as sketched in Figure 4:

- Type A hydrograph, showing a rapid rise followed by a global maximum, a decline and a plateau corresponding to the equilibrium breach discharge;
- Type B hydrograph, showing a rapid rise followed by a local maximum, a decline and a gradual rise towards an equilibrium or quasi-equilibrium breach discharge;

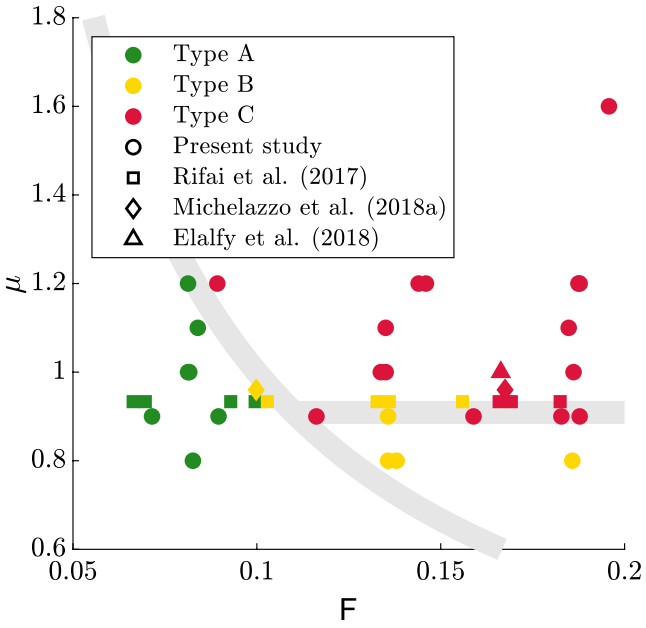

Figure 5. Occurrence of Types A, B, and C breach hydrographs in the present study as well as in experimental tests conducted by Rifai et al. (2017), Michelazzo, Oumeraci, and Paris (2018) and Elalfy et al. (2018) at laboratory scale. F represents the Froude number in the main channel. Colors refer to the breach hydrograph type, while the symbol shape indicates the data source. The gray-shaded lines represent the transition zones corresponding to $F \times \mu = 0.1$, and $\mu = 0.9$ ($F \times \mu > 0.1$).

- Type C hydrograph, showing a continuously increasing evolution towards an equilibrium or quasi-equilibrium breach discharge.

As detailed in Table S2 in Supplement, Type A hydrographs are mostly observed for a relatively low Froude number in the main channel (i.e., relatively low inflow discharge) and relatively weak dikes. In contrast, Type C hydrographs are obtained for a higher Froude number in the main channel and stronger dikes. This is confirmed by the distribution of the data points in the scatter plot displayed in Figure 5.

Figure 5 displays the results of the present tests and tests conducted in previous studies on the breaching of non-cohesive fluvial dikes along a straight main channel. Based on the available data, it appears that when the product $F \times \mu$ remains below ~0.1, the observed breach hydrographs tend to be of Type A. For larger values of $F \times \mu$, the type of hydrograph depends directly on the value of the normalized unit volume μ of the dike: for μ smaller than ~0.9, Type B hydrographs are mostly observed, whereas Type C hydrographs are obtained for μ above ~0.9. As can be seen in Figure 5, these transitions are not clear-cut, and the criteria based on F and μ should, at this stage of the research, be interpreted as representative of transition zones. The blurred nature of the transitions suggests that additional parameters may also control which type of breach hydrograph is obtained. The validity of the transition criteria beyond the range of values of F and μ tested here should be verified based on future tests exploring a broader range of variation for these parameters.

Overall, data tend to agree with the present classification based on the Froude number and geometric parameter μ. The occurrence of distinct patterns in the breach hydrographs reflects the co-existence of multiple time scales in the processes underpinning fluvial dike breaching. Hereafter, a simple conceptual model is introduced to explain the occurrence of the three types of breach hydrographs.

4.2. Multiplicity of Time Scales

The hydrodynamic process at stake during the failure of a fluvial dike can be seen as a combination of two extreme situations: the failure of an embankment dam, releasing the water from an upstream reservoir; and an open-channel system. We argue that a competition between these two aspects controls the pattern of the breach hydrograph. This competition depends on the relative magnitude of two characteristic time scales and on the dike strength (e.g., through parameter μ). In line with the concept of theoretical exposition depicted by Squazzoni et al. (2020), we describe hereafter a simple conceptual model, which has as sole objective to explore this theoretical explanation. The model was designed to be the simplest possible, while being able to reproduce the breach hydrograph typology. It is not intended to make predictions for real-world cases, since it is not able to grasp effects of many parameters, such as the main channel and floodplain geometry, the dike material and non-homogeneous features of real-world structures (lining, core), or the propagation of waves in the main channel.

Assuming the breach hydraulics is similar to that of a rectangular broad-crested weir, the mass balance for the main channel reads:

$$A\frac{dh}{dt} = \underbrace{Q_{\text{in}}}_{①} \underbrace{-C_b\ b\sqrt{g}\left(h-z\right)^{3/2}}_{②} \underbrace{-C_d\ b_{\text{mc}}\sqrt{g}\ h^{3/2}}_{③}, \tag{1}$$

with A the horizontal area of the main channel, h the water level in the main channel, C_b a discharge coefficient representative of the breach discharge capacity ($C_b \sim 0.5$), b the breach width (time-dependent), g the gravity acceleration, z the breach invert level (time-dependent), C_d a discharge coefficient representing the

channel downstream boundary condition, and b_{mc} the main channel width. The drain discharge is neglected in the present theoretical approach.

If terms ① and ③ are disregarded in Equation 1, then the left-hand-side together with the remaining term ② in the right-hand-side correspond to mass balance in case of a dam failure without inflow into the reservoir. In this case, a characteristic time scale of the process is $t_{c1} = A\ (g\ w^3)^{-1/2}$, since it enables writing the mass balance in the following simple form:

$$\frac{dH}{dT} = -C_b\ \ B\left(H - Z\right)^{3/2}, \tag{2}$$

with $H = h/w$ the non-dimensional water level, $B = b/w$ the non-dimensional breach width, $Z = z/w$ the non-dimensional breach invert level and $T = t/t_{c1}$ the non-dimensional time.

Similarly, if term ② is disregarded in Equation 1, and only terms ① and ③ are kept together with the left-hand-side, the remaining equation describes an open-channel system with inflow and outflow. In this case, another time scale emerges: $t_{c2} = A\ w/Q_{\text{in}}$, which is the residence time in main channel. It enables writing the mass balance in the following non-dimensional form:

$$\frac{dH}{dT'} = 1 - C_d \frac{\beta}{\alpha}\ \ H^{3/2}, \tag{3}$$

where $T' = t/t_{c2}$ is an alternate non-dimensional time, while $\beta = b_{\text{mc}}/w$ is a geometric parameter and $\alpha = Q_{\text{in}}/(g\ w^5)^{1/2}$ is a non-dimensional form for the main channel inflow discharge.

Based on these considerations, Equation 1 may be written in the following non-dimensional form:

$$\frac{dH}{dT} = \alpha - C_b\ \ B\left(H - Z\right)^{3/2} - C_d\ \ \beta\ \ H^{3/2}. \tag{4}$$

Note that parameter α is the ratio of time scales t_{c1} and t_{c2}. It reflects directly the relative magnitude of the time scales related to the "dam failure" component and to the "open-channel system" component of the flow processes of interest here. To solve Equation 4, we introduced a plausible assumption for the evolution of the non-dimensional breach invert level: $Z(T) = 1 - (1 + T^{-n})^{-1/n}$, as illustrated in Figure S7a in Supplement. The parameter n is adjusted to mimic the failure of dikes of various strengths (i.e., varying values of parameter μ). The breach width was assumed to grow as a multiple of the breach depth $1 - Z$ (Stage 1) and as a slowly increasing linear function of time (proxy for Stage 2): $B = m\ (1 - Z) + \gamma\ T$, with m and γ two model parameters. The evolution of B is illustrated in Figure S7b in Supplement. The representativity of the expressions used for $Z(T)$ and $B(T)$ was confirmed by a comparison with experimental data collected by Rifai et al. (2018, 2021). Equation 4 was solved with an explicit Runge-Kutta scheme and considering $H = 1$ as initial condition (i.e., water level at the dike crest).

To ensure flow equilibrium before breach development, $C_d\,\beta$ was set to the same value as α, in line with the "adjustment" of the boundary condition performed in the laboratory experiments to ensure that the water level in the main channel reaches the dike crest for each inflow discharge before breaching starts (Rifai et al., 2017, 2018). We set the remaining parameters to plausible values: $C_b = 0.5$, $m = 2$ and $\gamma = 0.05$, whereas parameter α was calculated from the three inflow discharges $Q_{in} = 25$ l/s, 40 l/s and 55 l/s, and from the dike height $w = 0.3$ m.

Figure 6 displays results for the three inflow discharges Q_{in}, leading to the following initial Froude numbers in the main channel: $F = 0.08$, $F = 0.13$ and $F = 0.18$ (see Table S1 in Supplement). It is amazing to see the similarity between the results of the simple conceptual model based on Equation 4 and the laboratory observations displayed in Figure 2. The different patterns followed by the breach hydrographs (e.g., occurrence or not of an absolute or relative maximum in the breach discharge) are fairly well reproduced by the conceptual model by changing only the inflow discharge, hence parameter α, and the strength of the dike (through parameter n). We believe that these results illustrate that the typology of breach hydrographs introduced in Section 4.1 is entirely controlled by the relative magnitude of the time scales related to the "dam failure" and the "open-channel system" flow processes, and by the dike strength. Hence, Type A hydrographs

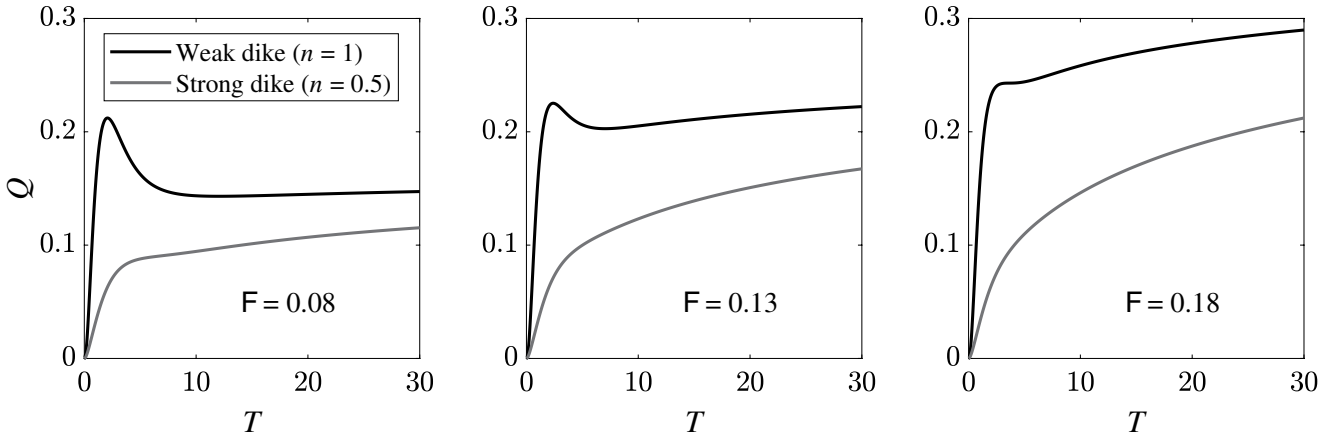

Figure 6. Non-dimensional breach hydrographs $Q(T) = C_b\, B\, (H - Z)^{3/2}$, computed by the conceptual model Equation 4 for the three inflow discharges considered in the laboratory experiments, corresponding to indicated initial Froude numbers F in the main channel.

correspond to a situation where the reservoir feature is prevalent while Type C hydrographs correspond to an open-channel system. For Type B hydrographs, both influences compete.

5. Conclusion

This paper examined the influence of dike geometry on the breach hydrograph and breach widening in the case of failure of homogeneous non-cohesive fluvial dikes due to overtopping at laboratory scale. The dike channel-side slope S_u, floodplain-side slope S_d and crest length L_k were varied systematically. The normalized unit dike volume μ was found to capture successfully the overall effect of these parameters.

The influence of dike geometry differs between Stage 1 (fast erosion) and Stage 2 (gradual evolution towards an equilibrium or quasi-equilibrium state) of breach expansion. During Stage 1, the gradient in breach discharge is milder for stronger dikes (i.e., larger μ), and this effect is magnified when the flow in the main channel is faster. Similarly, the breach expands more gently in both up- and downstream directions in the case of a stronger dike. In contrast, during Stage 2, the rate of breach expansion and outflow discharge are less influenced by the dike geometric parameters.

As the observed breach hydrographs follow three distinct patterns, we introduced a typology of breach hydrographs based on the occurrence or not of an absolute or relative maximum in the breach discharge. Such a maximum occurs mainly for relatively weak dikes (lower values of μ) and a relatively slow flow in the main channel. Our classifications based on the Froude number in the main channel and on the dike strength (through parameter μ) seems to agree with previous studies. Based on a simple conceptual model, we linked the breach discharge typology to the relative magnitude of time scales related to "dam failure" and "open-channel system" flow processes, and to the dike strength. Non-dimensional parameters that emerge from this model may prove useful to normalize breach hydrographs for specific stages of breach expansion. For quantitative predictions of real-world cases, more sophisticated models must be used (e.g., Elalfy et al., 2018; Wu, 2013).

In our tests, when we varied the channel-side slope of the dike, while keeping the inflow discharge unchanged in the main channel, we actually modified the flow velocity, Froude number and hence the momentum in the main channel. In the future, the specific effect of varying the channel-side slope of the dike could be isolated by means of experimental tests designed to preserve the Froude number in the main channel by adjusting the inlet discharge when the channel-side slope of the dike is varied.

Limitations of this study include a relatively narrow range of investigated Froude numbers in the main channel ($0.07 < F < 0.2$) and normalized unit dike volume (mostly $0.8 \leq \mu \leq 1.2$). The influence of main channel roughness and bottom erodibility was also not investigated, although the latter may play an important role in the breaching process. Though our experiments used comparatively larger dikes (0.30 m

in height) than in most previous research (0.10–0.20 m in height), scale effects may nonetheless affect the laboratory observations. Therefore, larger scale studies are needed, as well as laboratory experiments aiming at grasping the effects of other parameters such as non-homogeneous features of real-world dikes (lining, core).

Data Availability Statement

Data used in this article is available in the "Data Set S1" file (.h5 format).

Acknowledgments
The authors gratefully acknowledge B. Boucher, B. Coroenne, and N. Rousseau for their contribution to the experimental tests. They also express their gratitude to J. Walder and two anonymous Reviewers, whose detailed analysis and insightful comments have greatly improved this paper.

References

Aerts, J. C., Botzen, W. J., Clarke, K. C., Cutter, S. L., Hall, J. W., Merz, B., et al. (2018). Integrating human behaviour dynamics into flood disaster risk assessment. *Nature Climate Change*, *8*(3), 193–199. https://doi.org/10.1038/s41558-018-0085-1

Amaral, S., Caldeira, L., Viseu, T., & Ferreira, R. M. (2020). Designing experiments to study dam breach hydraulic phenomena. *Journal of Hydraulic Engineering*, *146*(4), 04020014. https://doi.org/10.1061/(asce)hy.1943-7900.0001678

ASCE/EWRI Task Committee on Dam/Levee Breaching. (2011). Earthen embankment breaching. *Journal of Hydraulic Engineering*, *137*(12), 1549–1564.

Bento, A. M., Amaral, S., Viseu, T., Cardoso, R., & Ferreira, R. M. (2017). Direct estimate of the breach hydrograph of an overtopped Earth dam. *Journal of Hydraulic Engineering*, *143*(6), 06017004. https://doi.org/10.1061/(asce)hy.1943-7900.0001294

Bhattarai, P. K., Nakagawa, H., Kawaike, K., & Zhang, H. (2015). Study of breach characteristics and scour pattern for overtopping induced river dyke breach. In *E-proceedings of the 36th IAHR world congress*.

Charrier, G. (2015). *Etude expérimentale des ruptures de digues fluviales par surverse. PhD thesis*. University of Aix-Marseille (in french).

Coleman, S. E., Andrews, D. P., & Webby, M. G. (2002). Overtopping breaching of noncohesive homogeneous embankments. *Journal of Hydraulic Engineering*, *128*(9), 829–838. https://doi.org/10.1061/(asce)0733-9429(2002)128:9(829)

Danka, J., & Zhang, L. M. (2015). Dike failure mechanisms and breaching parameters. *Journal of Geotechnical and Geoenvironmental Engineering*, *141*(9), 04015039. https://doi.org/10.1061/(asce)gt.1943-5606.0001335

Di Baldassarre, G., Kreibich, H., Vorogushyn, S., Aerts, J., Arnbjerg-Nielsen, K., Barendrecht, M., et al. (2018). Hess opinions: An interdisciplinary research agenda to explore the unintended consequences of structural flood protection. *Hydrology and Earth System Sciences*, *22*(11), 5629–5637. https://doi.org/10.5194/hess-22-5629-2018

Dou, S. T., Wang, D. W., Yu, M. H., & Liang, Y. J. (2014). Numerical modeling of the lateral widening of levee breach by overtopping in a flume with 180 bend. *Natural Hazards and Earth System Sciences*, *14*(1), 11–20. https://doi.org/10.5194/nhess-14-11-2014

Elalfy, E., Tabrizi, A. A., & Chaudhry, M. H. (2018). Numerical and experimental modeling of levee breach including slumping failure of breach sides. *Journal of Hydraulic Engineering*, *144*(2), 04017066. https://doi.org/10.1061/(asce)hy.1943-7900.0001406

El kadi Abderrezzak, K., Die Moran, A., Mosselman, E., Bouchard, J. P., Habersack, H., Lebert, F., & Aelbrecht, D. (2014). A physical, movable-bed model for non-uniform sediment transport, fluvial erosion and bank failure in rivers. *Journal of Hydro-environment Research*, *8*(2), 95–114. https://doi.org/10.1016/j.jher.2013.09.004

Faeh, R. (2007). Numerical modeling of breach erosion of river embankments. *Journal of Hydraulic Engineering*, *133*(9), 1000–1009. https://doi.org/10.1061/(asce)0733-9429(2007)133:9(1000)

Islam, M. (2012). *Study on levee breach and successive disasters in low-land through numerical and experimental approaches. PhD thesis*. Nagoya university (Japan).

Jandora, J., & Říha, J. (2008). *The failure of embankment dams due to overtopping*. Vutium.

Kakinuma, T., & Shimizu, Y. (2014). Large-scale experiment and numerical modeling of a riverine levee breach. *Journal of Hydraulic Engineering*, *140*(9), 04014039. https://doi.org/10.1061/(asce)hy.1943-7900.0000902

Kakinuma, T., Tobita, D., Yokoyama, H., & Takeda, A. (2013). Levee breach observation at Chiyoda experimental flume. In *Advances in river sediment research* (pp. 1013–1020). Kyoto, Japan.

LaRocque, L. A., Elkholy, M., Hanif Chaudhry, M., & Imran, J. (2013). Experiments on urban flooding caused by a levee breach. *Journal of Hydraulic Engineering*, *139*(9), 960–973. https://doi.org/10.1061/(asce)hy.1943-7900.0000754

Michelazzo, G., Oumeraci, H., & Paris, E. (2015). Laboratory study on 3D flow structures induced by zero-height side weir and implications for 1D modeling. *Journal of Hydraulic Engineering*, *141*(10), 04015023. https://doi.org/10.1061/(asce)hy.1943-7900.0001027

Michelazzo, G., Oumeraci, H., & Paris, E. (2018a). New hypothesis for the final equilibrium stage of a river levee breach due to overflow. *Water Resources Research*, *54*(7), 4277–4293. https://doi.org/10.1029/2017wr021378

Michelazzo, G., Paris, E., & Solari, L. (2018b). On the vulnerability of river levees induced by seepage. *Journal of Flood Risk Management*, *11*, S677–S686. https://doi.org/10.1111/jfr3.12261

Morris, M. W., Hassan, M. A. A. M., & Vaskinn, K. A. (2007). Breach formation: Field test and laboratory experiments. *Journal of Hydraulic Research*, *45*(1), 9–17. https://doi.org/10.1080/00221686.2007.9521828

Müller, C., Frank, P. J., & Hager, W. H. (2016). Dyke overtopping: Effects of shape and headwater elevation. *Journal of Hydraulic Research*, *54*(4), 410–422. https://doi.org/10.1080/00221686.2016.1170072

Orlandini, S., Moretti, G., & Albertson, J. D. (2015). Evidence of an emerging levee failure mechanism causing disastrous floods in Italy. *Water Resources Research*, *51*(10), 7995–8011. https://doi.org/10.1002/2015wr017426

Özer, I. E., van Damme, M., & Jonkman, S. N. (2020). Towards an International Levee Performance Database (ILPD) and its use for macro-scale analysis of levee breaches and failures. *Water*, *12*(1), 119.

Pickert, G., Weitbrecht, V., & Bieberstein, A. (2011). Breaching of overtopped river embankments controlled by apparent cohesion. *Journal of Hydraulic Research*, *49*(2), 143–156. https://doi.org/10.1080/00221686.2011.552468

Rifai, I., El Kadi Abderrezzak, K., Erpicum, S., Archambeau, P., Violeau, D., Pirotton, M., & Dewals, B. (2018). Floodplain backwater effect on overtopping induced fluvial dike failure. *Water Resources Research*, *54*(11), 9060–9073. https://doi.org/10.1029/2017wr022492

Rifai, I., El Kadi Abderrezzak, K., Erpicum, S., Archambeau, P., Violeau, D., Pirotton, M., & Dewals, B. (2019). Flow and detailed 3D morphodynamic data from laboratory experiments of fluvial dike breaching. *Scientific Data*, *6*, 53. https://doi.org/10.1038/s41597-019-0057-y

Rifai, I., El Kadi Abderrezzak, K., Hager, W. H., Erpicum, S., Archambeau, P., Violeau, D., et al. (2021). Apparent cohesion effects on overtopping induced fluvial dike breaching. *Journal of Hydraulic Research*, *59*(1), 75–87. https://doi.org/10.1080/00221686.2020.1714760

Rifai, I., Erpicum, S., Archambeau, P., Violeau, D., Pirotton, M., El Kadi Abderrezzak, K., & Dewals, B. (2017). Overtopping induced failure of noncohesive, homogeneous fluvial dikes. *Water Resources Research*, *53*(4), 3373–3386. https://doi.org/10.1002/2016wr020053

Rifai, I., Schmitz, V., Erpicum, S., Archambeau, P., Violeau, D., Pirotton, M., et al. (2020). Continuous monitoring of fluvial dike breaching by a laser profilometry technique. *Water Resources Research*, *56*, e2019WR026941. https://doi.org/10.1029/2019WR026941

Sadeghi, S., Hakimzadeh, H., & Babaeian Amini, A. (2020). Experimental investigation into outflow hydrographs of nonhomogeneous Earth dam breaching due to overtopping. *Journal of Hydraulic Engineering*, *146*(1), 04019049. https://doi.org/10.1061/(asce)hy.1943-7900.0001664

Schmocker, L., Frank, P. J., & Hager, W. H. (2014). Overtopping dike-breach: Effect of grain size distribution. *Journal of Hydraulic Research*, *52*(4), 559–564. https://doi.org/10.1080/00221686.2013.878403

Schmocker, L., & Hager, W. H. (2009). Modelling dike breaching due to overtopping. *Journal of Hydraulic Research*, *47*(5), 585–597. https://doi.org/10.3826/jhr.2009.3586

Schmocker, L., & Hager, W. H. (2012). Plane dike-breach due to overtopping: Effects of sediment, dike height and discharge. *Journal of Hydraulic Research*, *50*(6), 576–586. https://doi.org/10.1080/00221686.2012.713034

Squazzoni, F., Polhill, J. G., Edmonds, B., Ahrweiler, P., Antosz, P., Scholz, G., & Gilbert, N. (2020). Computational models that matter during a global pandemic outbreak: A call to action. *Journal of Artificial Societies and Social Simulation*, *23*(2). https://doi.org/10.18564/jasss.4298

Van Lanen, H. A., Laaha, G., Kingston, D. G., Gauster, T., Ionita, M., Vidal, J. P., et al. (2016). Hydrology needed to manage droughts: The 2015 European case. *Hydrological Processes*, *30*(17), 3097–3104. https://doi.org/10.1002/hyp.10838

Viero, D. P., D'Alpaos, A., Carniello, L., & Defina, A. (2013). Mathematical modeling of flooding due to river bank failure. *Advances in Water Resources*, *59*, 82–94. https://doi.org/10.1016/j.advwatres.2013.05.011

Vorogushyn, S., Merz, B., & Apel, H. (2009). Development of dike fragility curves for piping and micro-instability breach mechanisms. *Natural Hazards and Earth System Sciences*, *9*(4), 1383–1401. https://doi.org/10.5194/nhess-9-1383-2009

Vorogushyn, S., Merz, B., Lindenschmidt, K. E., & Apel, H. (2010). A new methodology for flood hazard assessment considering dike breaches. *Water Resources Research*, *46*, W08541. https://doi.org/10.1029/2009wr008475

Ward, P. J., de Ruiter, M. C., Mård, J., Schröter, K., Van Loon, A., Veldkamp, T., et al. (2020). The need to integrate flood and drought disaster risk reduction strategies. *Water Security*, *11*, 100070. https://doi.org/10.1016/j.wasec.2020.100070

Ward, P. J., Jongman, B., Aerts, J. C., Bates, P. D., Botzen, W. J., Loaiza, A. D., et al. (2017). A global framework for future costs and benefits of river-flood protection in urban areas. *Nature Climate Change*, *7*(9), 642–646. https://doi.org/10.1038/nclimate3350

Wei, H., Yu, M., Wang, D., & Li, Y. (2016). Overtopping breaching of river levees constructed with cohesive sediments. *Natural Hazards and Earth System Sciences*, *16*(7), 1541–1551. https://doi.org/10.5194/nhess-16-1541-2016

Wu, S., Yu, M., Wei, H., Liang, Y., & Zeng, J. (2018). Non-symmetrical levee breaching processes in a channel bend due to overtopping. *International Journal of Sediment Research*, *33*(2), 208–215. https://doi.org/10.1016/j.ijsrc.2017.09.007

Wu, W. (2013). Simplified physically based model of earthen embankment breaching. *Journal of Hydraulic Engineering*, *139*(8), 837–851. https://doi.org/10.1061/(asce)hy.1943-7900.0000741

Yu, M. H., Wei, H. Y., Liang, Y. J., & Zhao, Y. (2013). Investigation of non-cohesive levee breach by overtopping flow. *Journal of Hydrodynamics, Ser. B*, *25*(4), 572–579. https://doi.org/10.1016/s1001-6058(11)60398-4

Zhang, L., Peng, M., Chang, D., & Xu, Y. (2016). *Dam failure mechanisms and risk assessment*. John Wiley & Sons.